

Fusion Research, Moscow, U.S.S.R., 1973 (Joint Institute for Nuclear Research, Moscow, 1973), p. 105.

⁵F. F. Chen and C. Etievant, *Phys. Fluids* **13**, 687 (1970).

⁶Equation (2) is derived under the condition that the

rf field is traveling in the z direction. In the case of an axially standing field, Γ_{iz} is represented by Eq. (2) multiplied by $\cos^2 k_{\parallel} z$, apart from small nonresonant terms.

⁷John A. Decker *et al.*, *Phys. Fluids* **10**, 2442 (1967).

Evolution of Colliding Plasmas

Anthony L. Peratt

Maxwell Laboratories, Inc., San Diego, California 92123

and

James Green and Dale Nielsen^(a)

Institute for Plasma Research, Stanford University, Stanford, California 94305

(Received 17 March 1980)

Three-dimensional, electromagnetic computer simulations are presented showing the evolution of colliding columnar plasmas. The interaction leads to a spiral configuration during which radiation is emitted.

PACS numbers: 52.55.Dy, 52.55.Ez, 52.65.+z, 98.50.Eb

The behavior and interaction of colliding plasmas is a problem which has been under investigation for twenty-five years. The salient point of these investigations is that plasmas which are generated and fired at each other from plasma guns or sources do not merge and decay in a simple manner. Instead, a rather dramatic configurational transformation is observed during which the emission of radiation is recorded. Bostick^{1,2} first coined the term "plasmoid" to describe the magnetic-field-carrying structure which he observed and photographed. Figure 1 depicts time-resolved Kerr-cell photographs and illustrates the attraction/repulsion property of interacting plasmoids. The winding and dragging of the plasmoid's magnetic fields leads to the creation of a spiral formation.

Renewed interest in colliding plasmas is primarily due to two device-oriented research applications; fast plasma shutters for high-power glass lasers and radiation source emission from colliding exploding-wire plasmas in high-power pulseline generators. In the first case, a dense ($> 10^{21} \text{ cm}^{-3}$) propagating plasma produced from an exploding wire is used to shield the final output amplifiers from target-reflected laser light. In the second case, a load consisting of an array of exploding wires is strung between the anode and cathode of a multiterawatt generator diode. X-ray pinhole-camera photographs of the radiation from the colliding vaporized-wire plasmas

often show a distinct helical form. At times, dense plasma columns, or filaments, which are apparently those of the original wire plasmas,

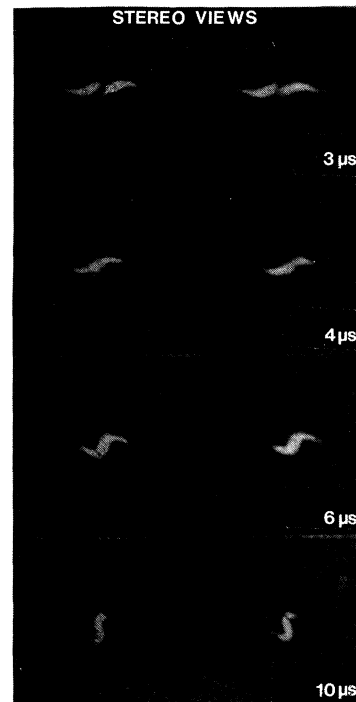


FIG. 1. Kerr-cell photographs of two plasmoids fired from sources 10 cm apart across a magnetic field of 4.7 kG (into paper) (Ref. 1).

are observed within the helix.³ In addition, less dense radial structure appears in the time-integrated x-ray photographs. We have observed the above phenomena in the collision of two wire plasmas, the minimum number required for interaction. A much reduced fluence is recorded when the load consists of a single wire.

Theoretical analyses of this problem are based upon the use of the virial theorem for deriving conditions of dynamical stability. This theorem was first used in magnetohydrodynamics by Chandrasekhar and Fermi to establish the condition for dynamic stability of cosmic gravitational masses balanced by gravitational, magnetic, and kinetic pressures.⁴ The basic geometry under consideration by Chandrasekhar and Fermi was cylindrical as was that of Shafranov,⁵ who extended the use of the theorem in order to investigate equilibrium configurations for current-carrying plasma columns. Shafranov has shown that the simplest equilibrium configuration in which the plasma pressure is taken up by a magnetic field is a cylindrical plasma pinch. Confinement is obtained by means of an azimuthally directed magnetic field resulting from electrical current flow through the plasma. In this case, the ther-

mokinetic force is balanced by the $\vec{j} \times \vec{B}$ force rather than the gravitation force. The stability of the equilibrium state of the plasma or the transition to an equilibrium state from a columnar state is treated by assuming a perturbation of the form $\xi = \xi(r) \exp i(k_z z + m\varphi - \omega t)$ where k_z and m are the axial and azimuthal wave numbers, respectively, and ω is the angular frequency of mode oscillation. Shafranov obtained a solution to the magnetostatic equations in terms of flux function, ψ , from which all other quantities may be derived (e.g., $p = p_0 + C_p \psi$, $I = I_0 + C_I \psi$, $B = B_0 + C_B \psi$, etc., where the subscript zero pertains to the unperturbed pressures, currents, and magnetic field and C_p , C_I , and C_B are constants). For an azimuthally symmetric configuration, $\psi(r, z)$ is

$$\psi = \bar{\psi} - C_p r^4 / 8\mu_0 - C_I r^2 (\frac{1}{2} \ln r - \frac{1}{4}), \quad (1)$$

$$\bar{\psi} = \frac{\sin(k_z z)}{\cos(k_z z)} r C_1(i k_z r),$$

where μ_0 is the free-space permeability and C_1 can be a linear combination of Bessel and Hankel functions of order 1, the type of which is determined by the boundary conditions imposed on $\bar{\psi}$. For an azimuthally asymmetric configuration $\psi(r, \varphi, z)$ is

$$\psi = \bar{\psi} - C_p r^2 (k_z^2 r^2 + 2m^2) / 8\mu_0 - C_I r^2 (\frac{1}{2} \ln r - \frac{1}{4}) + C (\frac{1}{2} k_z^2 r^2 + m^2 \ln r) - \frac{1}{2} k_z^2 I / m, \quad (2)$$

$$\bar{\psi} = \frac{\sin(k_z z)}{\cos(k_z z)} \frac{\sin(m\varphi)}{\cos(m\varphi)} r C_m'(k_z r) \quad (m \neq 0),$$

where C is an arbitrary constant. Contours of constant ψ , each of which represent surfaces of constant current and magnetic field, define the configuration, or plasmoids, form. We have generated these contours from Eqs. (1) and (2) and, for $m=0$, find nested toroids enclosed within spheroids. Thus, Eq. (1) predicts the existence of both toroidal and poloidal components of I and B within the plasma [Hill's vortex⁶ is recovered from Eq. (1) when $k_z \rightarrow 0$, $C_I = 0$, $C_p = 8\mu_0$, and $\bar{\psi}$ is a degenerate solution]. For $m=1$, helices (also having toroidal and poloidal components of I and B) are computed from Eq. (2). The transition to a state of dynamical equilibrium as represented by Eq. (1) or (2) by a cylinder unstable to a perturbation ξ generally occurs after the pinch perturbation has grown sufficiently large. This process begins after the current flowing through the column exceeds the Bennett current.⁷ Murty, in deriving instability growth rates, has found that a fluid cylinder is stable to all modes $m > 1$ when the axial current density is distributed

throughout the conducting volume.⁸ In the absence of an external magnetic field, the $m=0$ mode predominates, while when this field is present, there exists a critical product of axial current and longitudinal magnetic field which determines whether the $m=0$ or the $m=1$ mode will be manifested first among the possible instabilities.

When two such current-carrying plasma columns are present the Biot-Savart force due to parallel axial currents is attractive ($\propto -r^{-1}$) while the force between the counterparallel toroidal currents, due to column spin in the presence of an axial magnetic field, is repulsive ($\propto +r^{-3}$). The repulsive component of force is amplified after the pinch-induced equilibrium state is reached. In close proximity, the attractive and repulsive forces can be of comparable magnitude.^{9,10}

In the first three-dimensional fully electromagnetic simulation of a Z pinch, Nielsen, Green, and Buneman observed fluid behavior with the particle code SPLASH.^{11,12} In particular, they

found a rapid development of an $m = 1$ equilibrium with vortex behavior after the pinch of a columnar plasma immersed in a strong longitudinal magnetic field. The simulation here consists of two plasma columns of electrons and ions with Gaussianlike radial density profiles of width $10\lambda_D$ where λ_D is the Debye length. A large external magnetic field ($\beta = 3$ to 10%) is applied uniformly throughout the column and simulation region with the field lines parallel to the axis of the column. With regard to computer economy, the time scale of the evolution is speeded up as fast as resolution reasonably allows; the mass ratio is $m_i/m_e = 16$ and the electron temperatures are in the kiloelectronvolt range. A strong uniform electric field is applied so that the electrons and ions are accelerated in opposite directions. On the order of 100 000 particles were used in these simulations. The current was large enough to confine the plasma, but did not exceed the helical transition threshold. Single-frame photographs of the electrons are shown in Fig. 2.

Initially ($\omega_p t = 0$ where ω_p is the angular plasma frequency), two identical columns are placed

four radii between centers [Fig. 2(a)]. The columns spin in a counterclockwise (CCW) direction, a result of the z -directed magnetic field. The Biot-Savart force law for this initialization of fields dictates an interaction between the two columns whose cross sections are deformed into ellipses ($\omega_p t$ between 50 and 100). This interaction produces a bulk clockwise (CW) rotation of the "double-elliptical" pair which ultimately determines the CW rotation of the spiral. However, the CCW spin is retained by the columns throughout this stage of the transformation. As the columns elongate radially into a "head-tail" configuration, the spin becomes a CCW electron flow with faster electron velocities at the configuration surface. Beyond $\omega_p t = 300$, the configuration changes into a "barred spiral." The last frame in this sequence, $\omega_p t = 325$, shows the heretofore distinct plasmoids starting to coalesce at the center.

Figure 2(b) depicts frames from a movie of a simulation similar to that used to create a barred spiral except that the columns have been initially placed closer together so that the phenomenon associated with coalescence is stronger. Again, both columns spin in a CCW direction but eventually produce a spiral whose bulk motion is CW. Throughout this simulation, components of these individual spins may be identified within the structure but the interaction between these flows leads to some rather dramatic configuration transformations. When $\omega_p t$ is between 25 and 100, "two-discs-in-contact" to "irregular" to "figure-eight" or "dumbbell" forms are identifiable. Beyond $\omega_p t = 100$ the frames show a rather uniform but slowly evolving regular spiral.

Some of the behavior shown in Figs. 2(a) and 2(b) were anticipated from the earlier experimental and theoretical work. What was unexpected was the unusual clarity and insight given to understanding previous photographic data. The movies allow a frame-by-frame study of the particle dynamics and bulk cluster evolution that are unavailable by any other means. One unforeseen result was the rapid formation of spirals from colliding plasmoids.

In summary, we find that colliding plasmoids of circular cross section lead to configuration transformations and ultimately to spirals. The shape or type classification of these spirals are strongly influenced by the plasmoids' poloidal-toroidal magnetic field distribution.

One of the authors (A.L.P.) has benefitted from his associations with Professor H. Alfvén and Dr. J. W. Shearer. Two of the authors (J. G. and

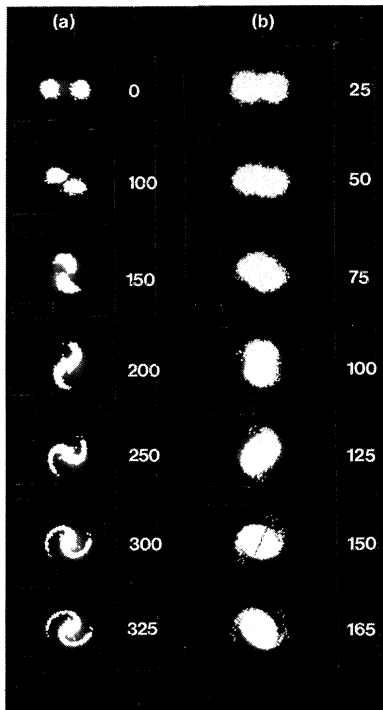


FIG. 2. Single-frame photographs of simulation electrons vs $\omega_p t$ (\hat{z} out of paper). (a) Initial plasma columns spaced four radii apart. (b) Initial plasma columns spaced two radii apart.

D. N. acknowledge the direction of Professor O. Buneman.

^(a)Present address: Lawrence Livermore Laboratory, Livermore, California 94550.

¹W. H. Bostick, Phys. Rev. 106, 404 (1957).

²W. H. Bostick, Phys. Rev. 104, 292 (1956).

³A. L. Peratt, M. Gersten, R. Richardson, and W. Clark, Bull. Am. Phys. Soc. 24, 1079 (1979).

⁴S. Chandrasekhar and E. Fermi, Astrophys. J. 118, 116 (1953).

⁵V. P. Shafranov, in *Reviews of Plasma Physics*, ed-

ited by M. A. Leontovich (Consultants Bureau, New York, 1966), Vol. 2.

⁶H. Lamb, *Hydrodynamics* (Dover Publications, New York, 1932), 6th ed., p. 233.

⁷W. H. Bennett, Phys. Rev. 45, 890 (1934).

⁸G. S. Murty, Ark. Fys. 19, 483 (1961).

⁹J. Davidson and D. R. Wells, Phys. Fluids 22, 379 (1979).

¹⁰S. Chandrasekhar, Proc. Natl. Acad. Sci. U. S. A. 42, 1 (1956).

¹¹D. E. Nielsen, Jr., Stanford University Institute for Plasma Research Report No. SU-IPR 776, 1979 (unpublished).

¹²D. Nielsen, J. Green, and O. Buneman, Phys. Rev. Lett. 42, 1974 (1979).

Ultrahigh-Vacuum Studies of Enhanced Raman Scattering from Pyridine on Ag Surfaces

J. E. Rowe, C. V. Shank, D. A. Zwemer, and C. A. Murray

Bell Laboratories, Murray Hill, New Jersey 07974, and Bell Laboratories, Holmdel, New Jersey 07733

(Received 3 March 1980)

Studies of surface-enhanced Raman scattering from pyridine adsorbed on Ag surfaces in ultrahigh vacuum show a strong dependence on both surface roughness and pyridine coverage. The observation of enhancement (10^4) for physisorbed pyridine multilayers in addition to the first molecular layer implies that the enhanced effect is electromagnetic rather than chemical in origin.

PACS numbers: 78.30.Jw

Recent observations of Raman scattering from adsorbed molecules near Ag surfaces have been interpreted in terms of a giant enhancement ($\sim 10^4 - 10^6$) of the Raman cross section of molecules in the first monolayer in contact with the Ag surface. These experiments have been performed with solid-solid interfaces¹ (i.e., tunnel-junction geometries), solid-liquid interfaces² (i.e., electrochemical cells), and more recently solid-vacuum studies in ultrahigh vacuum (UHV).³ The last geometry has some specific advantages because of the possibilities of *in situ* surface characterization and continuous variation of surface coverage. Both of these features are important to test several of the proposed theoretical mechanisms of the surface-enhanced Raman effect. We have studied surface-enhanced Raman scattering (SERS) by performing UHV measurements on a variety of Ag surfaces characterized by Auger-electron spectroscopy (AES) and low-energy electron diffraction (LEED). Both surface-roughness and adsorbate-coverage dependences have been measured which suggest that the dominant contribution to SERS is electromagnetic rather than

chemical in origin.

The apparatus used for Raman measurements was a multiple-technique UHV chamber which has been previously described.⁴ The Raman scattering was performed primarily with the 4880-Å line from an Ar-ion laser although some measurements were also performed at 5145 and 4965 Å to verify the inelastic scattering nature of the main features observed. The laser light was directed at the Ag sample at $\theta_1 = 65^\circ$ angle of incidence; it was *p* polarized and the scattered light was collected in a $\sim 40^\circ$ cone near the surface normal. This geometry is similar to that previously used in most electrochemical cell experiments. The scattered light was analyzed by a double-grating spectrometer and photon counting detection operated with a resolution typically $\sim 8 \text{ cm}^{-1}$.

Pyridine was deposited with sample temperature $T \approx 135 \text{ K}$ by filling the experimental chamber with pyridine vapor to a pressure $10^{-7} - 10^{-6}$ Torr and the coverage was determined from condensation kinetics measured by AES measurements at a pressure of 10^{-9} Torr.⁵ Figure 1

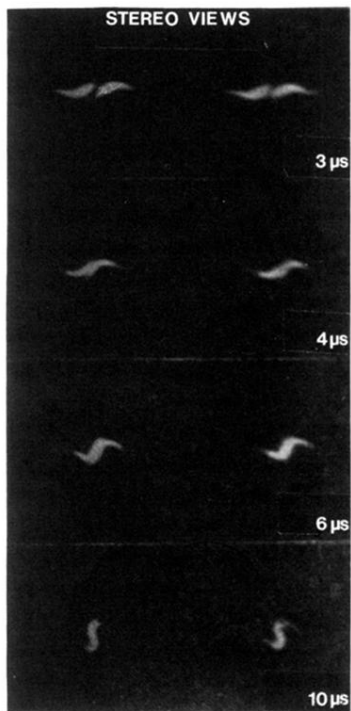


FIG. 1. Kerr-cell photographs of two plasmoids fired from sources 10 cm apart across a magnetic field of 4.7 kG (into paper) (Ref. 1).

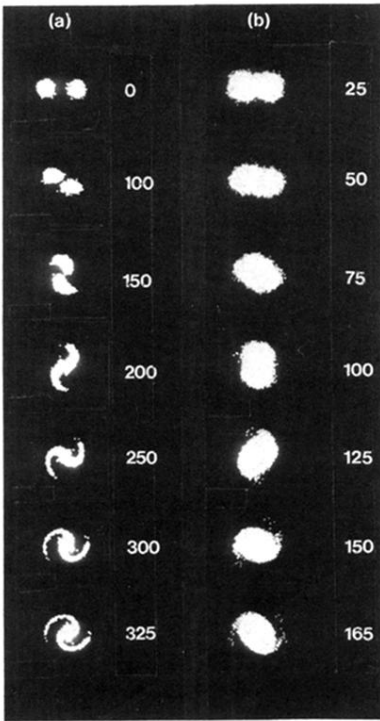


FIG. 2. Single-frame photographs of simulation electrons vs $\omega_p t$ (\hat{z} out of paper). (a) Initial plasma columns spaced four radii apart. (b) Initial plasma columns spaced two radii apart.